

# Lepton-Charge and Forward-Backward Asymmetries in Drell-Yan Processes for Precision Electroweak Measurements and New Physics Searches

J. Fiaschi\*

*Department of Mathematical Sciences, University of Liverpool, Liverpool L69 3BX, United Kingdom*

F. Giuli

*CERN, CH 1211 Geneva*

*University of Rome Tor Vergata and INFN, Sezione di Roma 2, Via della Ricerca Scientifica 1, 00133 Roma*

F. Hautmann

*Elementaire Deeltjes Fysica, Universiteit Antwerpen, B 2020 Antwerpen*

*Theoretical Physics Department, University of Oxford, Oxford OX1 3PU*

S. Moretti

*School of Physics and Astronomy, University of Southampton, Highfield, Southampton SO17 1BJ, UK*

---

## Abstract

Precision determinations of Standard Model (SM) Electro-Weak (EW) parameters at the Large Hadron Collider (LHC) are dominated by uncertainties due to Parton Distribution Functions (PDFs). Reweighting and profiling techniques are routinely employed to treat this. We explore approaches based on combining measurements of charged current and neutral current Drell-Yan (DY) asymmetries to improve PDF uncertainties. We present the results of a numerical analysis performed with the open-source platform `xFitter`. PDF uncertainties are examined for lepton-charge and forward-backward asymmetries in regions of transverse and invariant masses near the vector-boson peak, based on LHC Run III and HL-LHC luminosity scenarios. We discuss the complementarity of the asymmetries in reducing PDF uncertainties in observables relevant to both SM and Beyond the SM (BSM) physics.

---

\*Corresponding author

*Email addresses:* `fiaschi@liverpool.ac.uk` (J. Fiaschi),  
`francesco.giuli@roma2.infn.it`, `francesco.giuli@cern.ch` (F. Giuli),  
`hautmann@thphys.ox.ac.uk` (F. Hautmann), `s.moretti@soton.ac.uk` (S. Moretti)

*Keywords:*

LTH 1259,

arXiv:2103.10224,

Electroweak interaction, Lepton production, QCD Phenomenology, Beyond Standard Model

---

## 1. Introduction

The LHC, having completed its Runs I and II, has recently provided determinations of the weak mixing angle  $\theta_W$  [1, 2, 3] and  $W$  boson mass  $m_W$  [4, 5] which are competitive in accuracy with previous determinations from lepton colliders [6] and Tevatron [7, 8]. The quest for ever increasing accuracy in precision measurements of EW parameters of the SM will continue to be at the center of the physics programme in forthcoming LHC runs and at the High-Luminosity LHC (HL-LHC) [9], including the proposed Large Hadron-electron Collider (LHeC) option [10].

The dominant uncertainties on current determinations of  $m_W$  and  $\theta_W$  at the LHC come from non-perturbative contributions due to the hadron structure in the initial state [11, 12]. In the framework of QCD collinear hard-scattering factorisation for inclusive  $pp$  production processes [13], such contributions are embodied in quark and gluon PDFs. The successful completion of the precision EW physics programme at the LHC and HL-LHC thus calls for careful scrutiny of the PDFs, including understanding their correlations with the measured EW parameters, the associated uncertainties as well as looking for methods to improve the latter.

Given this source of uncertainties, current ATLAS and CMS analyses carry out EW measurements so that PDFs are constrained in-situ by profiling and reweighting techniques. An example is provided by the determinations of  $\theta_W$  in [1, 2] through DY measurements. The CMS analysis of Ref. [1] uses the reweighting technique to constrain PDF uncertainties while profiling of PDF error eigenvectors is used as a cross-check. In the ATLAS note [2] the PDF uncertainties are instead included in the likelihood fit and thus constrained.

Alternative strategies focus on looking for new measurements, capable of providing high sensitivity to PDFs with low theoretical and experimental systematics while controlling correlations. An example is provided by the analysis [14] of the neutral current DY Forward-Backward Asymmetry  $A_{FB}$  in the `xFitter` framework [15]. In the  $Z$  boson resonance region the  $A_{FB}$  observable is exploited to measure the weak mixing angle  $\theta_W$  and it is sensitive to the charge-weighted linear combination  $(2/3)u_V + (1/3)d_V$  of up-quark and down-quark PDFs [14, 16] through the  $Z/\gamma$  interference away from the resonance. It can thus be used to constrain quark PDFs [17, 18, 19] while additional observables are needed to achieve flavour decomposition.

The purpose of this work is to extend the investigation in [14] by using the charged current lepton-charge asymmetry  $A_W$  in combination with  $A_{FB}$  and study the implications of the combined analysis on PDF uncertainties. We will

exploit the sensitivity of the lepton-charge asymmetry  $A_W$  to the difference  $u_V - d_V$  to probe linearly independent combinations of up-quark and down-quark PDFs from both  $A_{FB}$  and  $A_W$ .

We will consider measurements of lepton-charge asymmetry at Runs I and II [20, 21] as well as future measurements at Run III and HL-LHC luminosities.

Studies of the impact of  $W$  and  $Z$  production data on PDFs have recently appeared [22, 23] based on the EPUMP package [24, 25, 26].

The paper is organised as follows. In Sec. II we describe the calculational framework for DY asymmetries in `xFitter` and validate it by comparing Next-to-Leading-Order (NLO) results with Run I experimental data. In Sec. III we consider Run III and HL-LHC luminosities and perform a PDF profiling calculation. Using `xFitter`, we analyze the separate and combined impact of high-statistics  $A_{FB}$  and  $A_W$  asymmetry measurements in the mass region near the vector boson pole on PDF uncertainties. In Sec. IV we illustrate the implications of this analysis for various DY observables, discussing examples both in the region of SM vector boson masses and in the multi-TeV region relevant for new physics BSM searches. We give our conclusions in Sec. V.

## 2. xFitter calculational framework and comparison with Run I data

We here recall the main elements of the `xFitter` [15] calculational framework applied to the DY lepton-charge asymmetry  $A_W$ , defined as

$$A_W = \frac{d\sigma/d|\eta_\ell|(W^+ \rightarrow \ell^+\nu) - d\sigma/d|\eta_\ell|(W^- \rightarrow \ell^-\bar{\nu})}{d\sigma/d|\eta_\ell|(W^+ \rightarrow \ell^+\nu) + d\sigma/d|\eta_\ell|(W^- \rightarrow \ell^-\bar{\nu})}, \quad (1)$$

and to the reconstructed DY neutral forward-backward asymmetry  $A_{FB}$ , defined as

$$A_{FB} = \frac{d\sigma/dM_{\ell\ell}(\cos\theta^* > 0) - d\sigma/dM_{\ell\ell}(\cos\theta^* < 0)}{d\sigma/dM_{\ell\ell}(\cos\theta^* > 0) + d\sigma/dM_{\ell\ell}(\cos\theta^* < 0)}, \quad (2)$$

where  $\eta_\ell$  is the pseudorapidity of the charged lepton defined in the laboratory frame,  $M_{\ell\ell}$  is the di-lepton system invariant mass and  $\theta^*$  is the angle between the outgoing lepton and the incoming quark defined in the Collins–Soper frame [27].

We validate the implementation of  $A_W$  by performing fits to ATLAS experimental data [20] at  $\sqrt{s} = 8$  TeV. The observable has been computed at NLO in perturbative QCD, using the `MadGraph5_aMC@NLO` [28] program, interfaced to `APPLgrid` [29] through `aMCfast` [30]. We obtain theoretical predictions corresponding to the analysis cuts of the ATLAS data recorded at  $\sqrt{s} = 8$  TeV from Ref. [20]. The renormalisation and factorisation scales  $\mu_R$  and  $\mu_F$  in the NLO computations are set equal to  $\mu_R = \mu_F = m_W$ .

These computations are supplemented by  $K$ -factors to match theoretical predictions from an optimised version of the `DYNNLO` generator [31], which simulates initial-state QCD corrections to Next-to-NLO (NNLO) accuracy, at LO in the EW couplings with parameters set according to the  $G_\mu$  scheme [32]. The input parameters (the Fermi constant  $G_F$ , the masses and widths of the  $W$  and

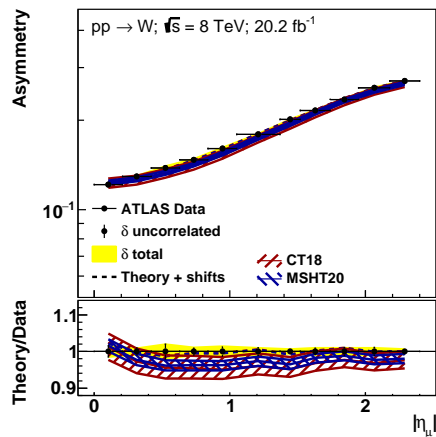


Figure 1: Muon rapidity dependence of the lepton-charge asymmetry  $A_W$ , for CT18NNLO [34] and MSHT20 [35] PDFs, compared with the ATLAS measurements [20] at  $\sqrt{s} = 8$  TeV.

PDF set	$\chi^2/\text{d.o.f.}$
CT18NNLO	10.26/11
CT18ANNLO	11.29/11
MSHT20nnlo_as118	12.18/11
NNPDF3.1_nnlo_as_0118_hessian	14.88/11
PDF4LHC15_nnlo_100	9.53/11
ABMP16_5_nnlo	18.21/11
HERAPDF20_NNLO_EIG	8.92/11

Table 1: The  $\chi^2$  values per degree of freedom from fits to  $A_W$  experimental measurements [20] using `xFitter` [15], for different PDF sets. PDF uncertainties are evaluated at the 68% Confidence Level (CL).

$Z$  bosons and the Cabibbo-Kobayashi-Maskawa (CKM) entries) are taken from Ref. [33].

In Fig. 1 we implement the calculation of  $A_W$  in `xFitter` [15] and present the comparison of our theoretical predictions for  $A_W$  (for two choices of PDFs, CT18NNLO [34] and MSHT20nnlo [35]) with the ATLAS experimental measurements [20]. In Tab. 1 we extend the comparison by performing fits with several PDF sets: CT18NNLO, CT18ANNLO [34], MSHT20nnlo [35], NNPDF3.1nnlo [36], PDF4LHC15nnlo [37], ABMP16nnlo [38] and HERAPDF2.0nnlo [39]. The results for the  $\chi^2$  values are reported in Tab. 1 for each of the PDF sets, showing a good description of data for all sets.

We investigate the accuracy of our computation for  $A_W$  by estimating its theory uncertainty through variation of the factorisation and renormalisation scales. Fig. 2 shows  $A_W$  theoretical predictions versus  $W$ -boson rapidity at

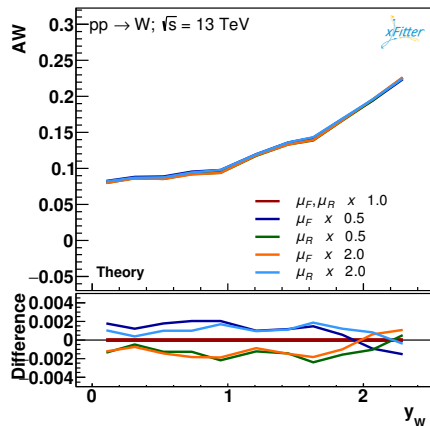


Figure 2:  $W$ -boson rapidity dependence of the lepton-charge asymmetry  $A_W$  for different choices of factorisation and renormalisation scales.

$\sqrt{s} = 13$  TeV, where the factorisation and renormalisation scales are varied by a factor 2 or 0.5. The differences with respect to the  $A_W$  central value curve ( $\mu_F$  and  $\mu_R$  unchanged) are at the permille level, thus confirming the reliability of the calculations with respect to this systematic uncertainty.

### 3. Complementarity of $A_{FB}$ and $A_W$

In this section we extend the profiling analysis [14] of  $A_{FB}$  by using  $A_W$  in combination with  $A_{FB}$ , and study the implications of the combined analysis on PDF uncertainties. We generate  $A_{FB}$  and  $A_W$  pseudodata at  $\sqrt{s} = 13$  TeV with integrated luminosities of 300 and 3000  $\text{fb}^{-1}$ , corresponding respectively to the designed values at the end of the LHC Run III and at the end of the HL-LHC.

We employ pseudodata for  $A_{FB}$  in the mass region around the  $Z$  peak, and pseudodata for  $A_W$  in the mass region around the  $W$  Jacobian peak. We compute  $A_W$  as described in Sec. 2. For  $A_{FB}$  we carry out an analogous calculation as described in Ref. [14]. We adopt the analysis cuts of the ATLAS  $A_{FB}$  measurements [40] at  $\sqrt{s} = 8$  TeV, in the invariant mass interval  $45 \text{ GeV} \leq M_{\ell\ell} \leq 200 \text{ GeV}$  using 61 bins of 2.5 GeV width, and set the  $\mu_R$  and  $\mu_F$  scales to the invariant mass of the dilepton pair in the final state, namely,  $\mu_R = \mu_F = m_{\ell\ell}$ . We project the statistical error on these observables for the luminosity scenarios considered by combining the statistics of electron and muon channels.

Following the method of Refs. [14, 41], we apply the technique [42, 43] to evaluate PDF uncertainties. The results will be shown at the chosen representative energy scale  $Q^2 = M_Z^2 = 8317 \text{ GeV}^2$ . We have checked that the qualitative behavior of the profiled distributions does not change when varying the  $Q^2$  values.

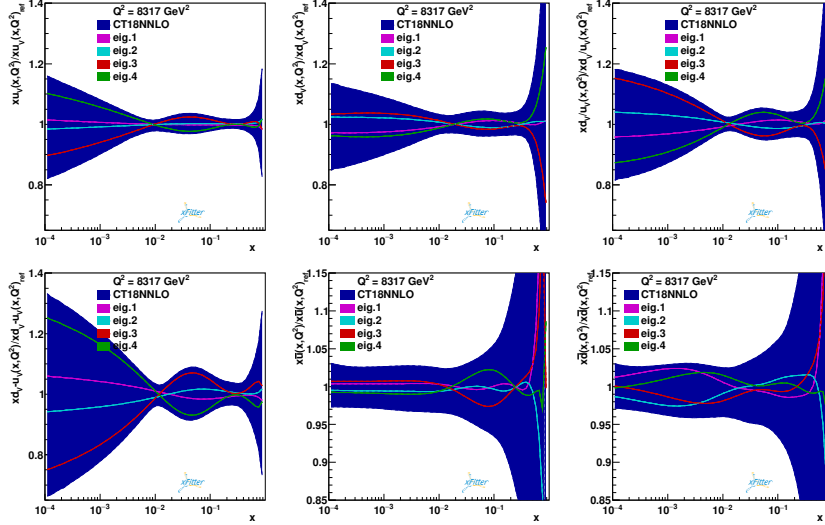


Figure 3: Contribution of rotated eigenvectors to the various PDFs.

### 3.1. Eigenvector rotation

We first want to identify the PDFs and their combinations which are most sensitive to the  $A_W$  observable, by performing an eigenvector rotation exercise analogous to that done for the case of  $A_{FB}$  in Ref. [14]. Using this technique [44], we rotate and sort the eigenvectors of the CT18NNLO PDF set according to the  $A_W$  pseudodata's impact on them, and plot the contribution of the first 4 eigenvectors to the error bands of different PDFs and their combinations.

Fig. 3 shows that the third and fourth eigenvectors provide the largest contribution to quark PDFs, while the first two eigenvectors have a comparable weight to the third and the fourth in the anti-quark PDFs. The saturation given by the first four eigenvectors on the error bars of the PDF composition  $d_V - u_V$  confirms that the  $A_W$  observable is most sensitive to this combination, and similar conclusion can be drawn on the PDF ratio  $d_V/u_V$ . In the following, we will then show the results of the profiling on these PDF distributions as well.

### 3.2. Profiling with $A_{FB}$ and $A_W$ separately

We show here the reduction of PDF error bands when  $A_{FB}$  and  $A_W$  pseudodata separately are used in the profiling. The constraints placed by  $A_{FB}$  and  $A_W$  on the valence quark PDFs are shown in Fig. 4. We note that the reduction of the error bands given by the two observables are comparable, with  $A_{FB}$  providing slightly stronger constraints.

Fig. 5 shows the constraints on the anti-quark distributions and we observe that here the constraints by  $A_W$  are slightly stronger than the ones from  $A_{FB}$ ,

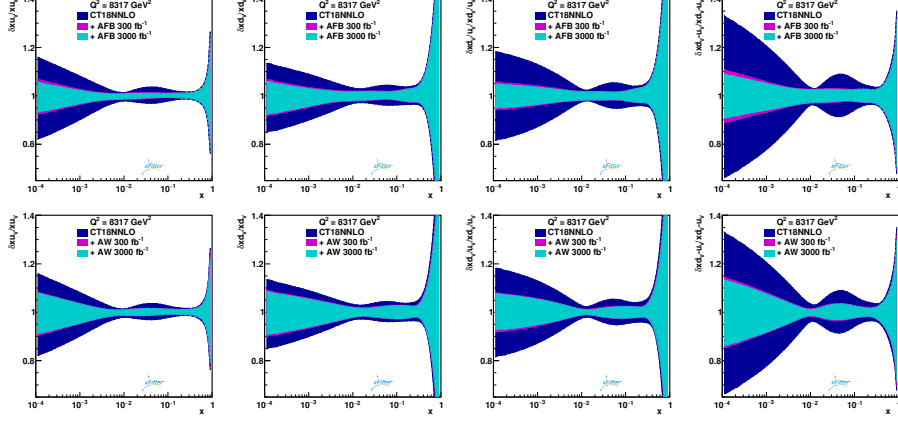


Figure 4: Original CT18NNLO [34] (blue) and profiled distributions using  $A_{FB}$  (top) and  $A_W$  (bottom) pseudodata corresponding to integrated luminosities of  $300 \text{ fb}^{-1}$  (pink) and  $3000 \text{ fb}^{-1}$  (cyan). Results are shown for valence quark distributions at  $Q^2 = M_Z^2 = 8317 \text{ GeV}^2$ .

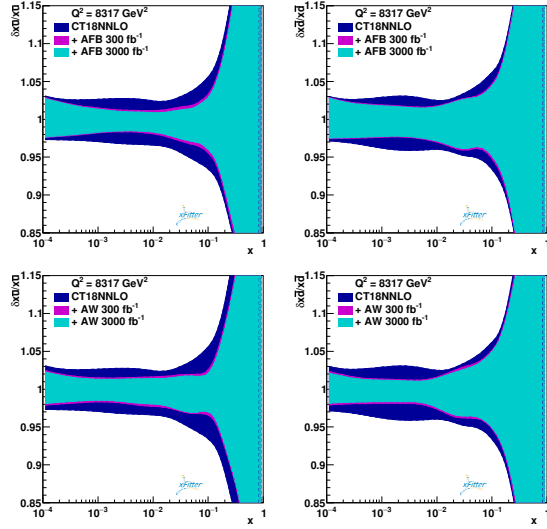


Figure 5: Original CT18NNLO [34] (blue) and profiled distributions using  $A_{FB}$  (top) and  $A_W$  (bottom) pseudodata corresponding to integrated luminosities of  $300 \text{ fb}^{-1}$  (pink) and  $3000 \text{ fb}^{-1}$  (cyan). Results are shown for anti-quark distributions.

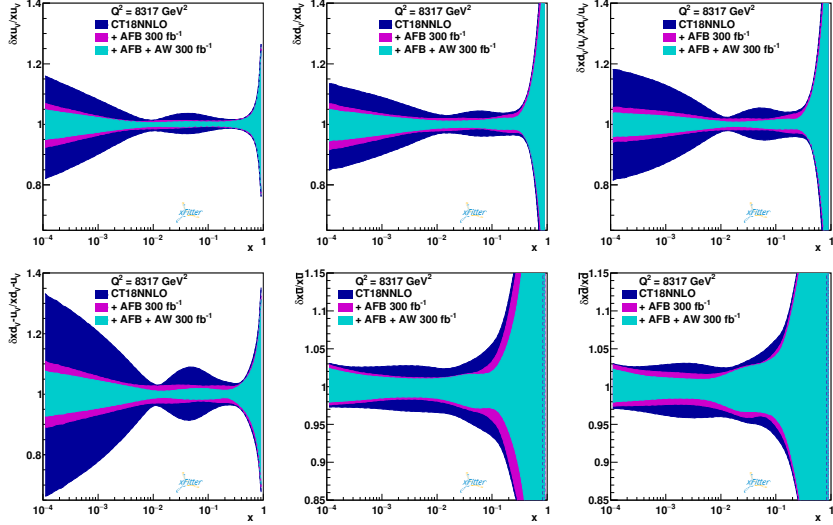


Figure 6: Original CT18NNLO [34] (blue) and profiled distributions using either  $A_{FB}$  (pink) or both  $A_{FB}$  and  $A_W$  (cyan) pseudodata corresponding to integrated luminosity of  $300 \text{ fb}^{-1}$ . Results are shown for valence-quark and sea-quark distributions at  $Q^2 = M_Z^2 = 8317 \text{ GeV}^2$ .

particularly for the  $\bar{u}$  PDF in the low  $x$  region and for the  $\bar{d}$  PDF in the low and intermediate  $x$  range. The improvement in this case is however more moderate.

We note that in the above results the reduction in PDF uncertainties appears to saturate with increasing luminosity, with the profiled error bands obtained for  $3000 \text{ fb}^{-1}$  being close to the ones obtained for  $300 \text{ fb}^{-1}$ .

### 3.3. Profiling with the combination of $A_{FB}$ and $A_W$

We next present the results of the profiling when superimposing constraints from  $A_{FB}$  and  $A_W$  pseudodata. Fig. 6 shows the profiled PDF set uncertainty bands using  $A_{FB}$  pseudodata, and the corresponding bands upon inclusion of constraints from  $A_W$  pseudodata, in the scenario of  $300 \text{ fb}^{-1}$  integrated luminosity. This illustrates how the combination of  $A_{FB}$  and  $A_W$  further improves PDF behaviour in terms of error reduction. For instance, in the  $d_V - u_V$  PDF combination at  $x = 10^{-4}$ , a 20% reduction of uncertainty from  $A_{FB}$  pseudodata is further improved by an extra 2% by the inclusion of the  $A_W$  observable.

Fig. 7 shows the analogous results in the scenario of  $3000 \text{ fb}^{-1}$  integrated luminosity. The saturation in the reduction of uncertainties already observed in the previous subsection is also visible here. Considering the  $d_V - u_V$  PDF combination at  $x = 10^{-4}$ , we observe a further reduction of about 1% with respect to the case with pseudodata corresponding to  $300 \text{ fb}^{-1}$  luminosity, when superimposing  $A_{FB}$  and  $A_W$  constrains.



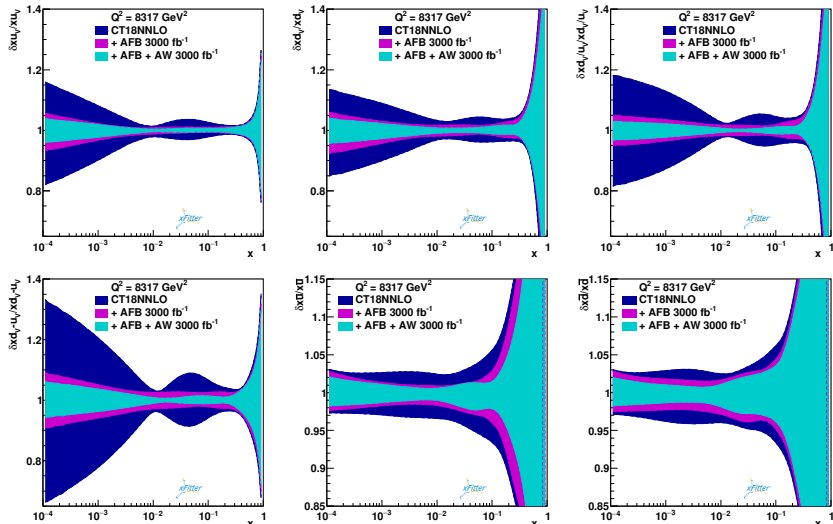


Figure 7: Same as in Fig. 6 but for integrated luminosity of  $3000 \text{ fb}^{-1}$ .

### 3.4. Antimatter asymmetry in the proton

In Fig. 8 we compare the improved PDF uncertainties, after profiling based on the combination of  $A_{FB}$  and  $A_W$  asymmetries, with the recent SeaQuest/E906 results [45], wherein it was shown that the ratio of the PDFs of  $\bar{d}$  and  $\bar{u}$  states as a function of  $x$  is notably different from both the QCD expectation of it being nearly 1 [46] and the predictions of several proposed mechanisms (e.g., Pauli blocking, statistical models, chiral solitons and meson-baryon dynamics) that had been disfavoured by similar previous results from NuSea/E866 [47]. The reduction in the PDF uncertainties in presence of  $A_{FB}$  and (especially)  $A_W$  constraints is significant, of up to a factor 2 in the very high  $x$  region, to the extent that data over the latter are no longer within the PDF errors, no matter the actual values of  $Q^2$  and luminosity considered. We remark that however in order to produce these results we have employed pseudodata projecting future LHC run statistics. The inclusion of future real data would likely modify the central values of the PDF distributions as well.

## 4. DY production at the EW mass scale and at TeV masses

In this section we present examples illustrating the implications of the analysis in Sec. 3 for DY observables both in the mass region near the SM vector-boson masses and in the multi-TeV mass region relevant for BSM searches.

### 4.1. PDF uncertainties in dilepton observables

We here examine theoretical uncertainties on dilepton observables due to the original PDF sets and the profiled sets obtained after imposing constraints from

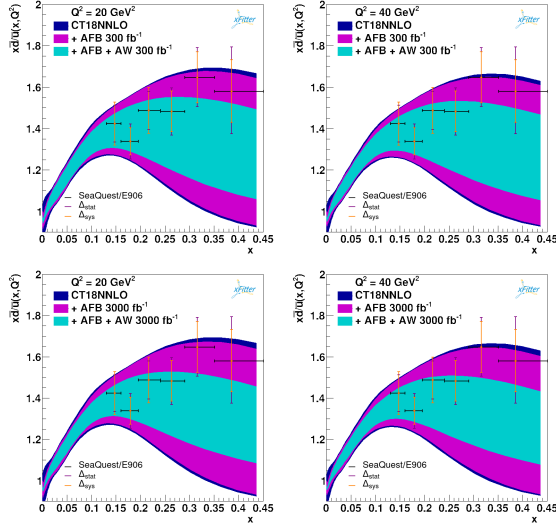


Figure 8: Profiled error bands with  $A_{FB}$  and  $A_W$  asymmetries for the  $\bar{d}/\bar{u}$  ratio of PDFs corresponding to 300 (top) and 3000 (bottom)  $\text{fb}^{-1}$  at the energy scales  $Q^2 = 20 \text{ GeV}^2$  (left) and  $Q^2 = 40 \text{ GeV}^2$  (right). The SeaQuest/E906 [45] results are superimposed for comparison.

$A_{FB}$  and  $A_W$  asymmetry measurements both with  $300 \text{ fb}^{-1}$  and  $3000 \text{ fb}^{-1}$  of luminosity.

While the best  $Z$ -boson mass determinations come from  $e^+e^-$  experimental data, the LHC provides competitive determinations of  $W$ -boson mass [4, 5]. Motivated by this, we start by considering the transverse mass spectrum and lepton transverse momentum spectrum of the charged DY channel.

Fig. 9 on the left shows the charged-current DY transverse mass spectrum with the relative PDF uncertainty bands obtained by the baseline CT18NNLO (rescaled at 68% CL) and by the profiled PDF set using the combination of  $A_{FB}$  and  $A_W$  measurements corresponding to  $300 \text{ fb}^{-1}$  of integrated luminosity, while on the right the ratio is shown for the profiled PDF error over the original one. The original PDF uncertainty in this region varies between 1.7% and 1.9%. The inclusion of  $A_{FB}$  constraints at 300 (3000)  $\text{fb}^{-1}$  reduces the uncertainty by about 12% (16%) while the inclusion of  $A_W$  constraints at 300 (3000)  $\text{fb}^{-1}$  reduces the uncertainty by about 26% (43%). By combining the two sets of constraints at 300 (3000)  $\text{fb}^{-1}$  the original PDF error bands are reduced by about 28% (46%).

Fig. 10 shows analogous results for the lepton transverse momentum spectrum. Again the original CT18NNLO (rescaled at 68% CL) PDF uncertainty ranges between 1.7% and 1.9% and its reduction obtained via asymmetry profiling has a similar behaviour to that obtained for the transverse mass distribution.

We next consider applications of our studies to the multi-TeV region, relevant for new physics searches, e.g, for new  $Z'$  and  $W'$  heavy boson states. In Fig. 11

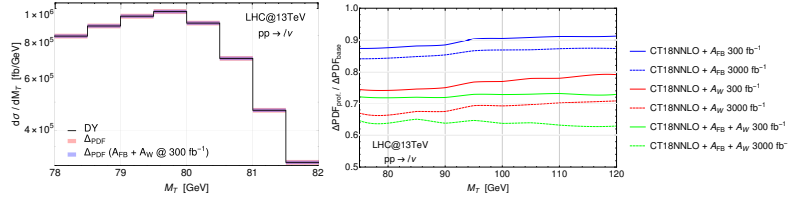


Figure 9: (left) Charged-current DY transverse mass distribution with PDF error; (right) relative improvement of PDF error on the transverse mass spectrum due to profiling based on  $A_{FB}$ ,  $A_W$  and their combination.

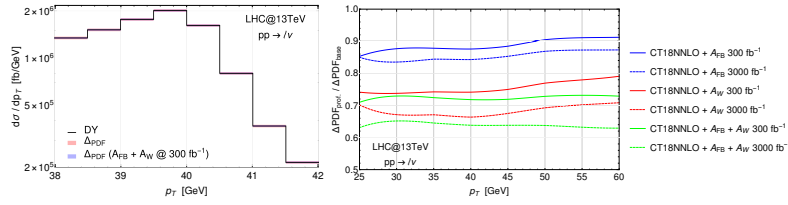


Figure 10: (left) Lepton transverse momentum distribution with PDF error; (right) relative improvement of PDF error on the lepton transverse momentum spectrum due to profiling based on  $A_{FB}$ ,  $A_W$  and their combination.

on the left we can observe the relative PDF error in the dilepton invariant mass distribution. The black curve represents the baseline CT18NNLO uncertainty while the coloured curves are the PDF errors after the profiling using the  $A_{FB}$  (blue curves) and  $A_W$  (red curves) measurements and their combination (green curves), corresponding to integrated luminosities of 300 fb $^{-1}$  (solid curves) and 3000 fb $^{-1}$  (dashed curves).  $A_{FB}$  reduces the PDF relative uncertainty from 5% to 3.8% (3.2%) for an invariant mass of 2 TeV and from 12% to 11% (10.2%) for an invariant mass of 4 TeV when using an integrated luminosity of 300 (3000) fb $^{-1}$ .  $A_W$  is able to reduce the PDF relative uncertainty to 3.4% (3.2%) for an invariant mass of 2 TeV and to 9.6% (9.4%) for an invariant mass of 4 TeV when using an integrated luminosity of 300 (3000) fb $^{-1}$ . The combination of  $A_{FB}$  and  $A_W$  further constrains the PDF relative uncertainty to 2.7% (2.3%) for an invariant mass of 2 TeV and to 8.4% (7.8%) for an invariant mass of 4 TeV when using an integrated luminosity of 300 (3000) fb $^{-1}$ .

In Fig. 11 on the right, the analogous analysis is presented for the charged DY channel in the transverse mass spectrum. The black curve represents the baseline CT18NNLO uncertainty while the coloured curves are the PDF errors after the profiling using the  $A_{FB}$  (blue curves) and  $A_W$  (red curves) measurements and their combination (green curves), corresponding to integrated luminosities of 300 fb $^{-1}$  (solid curves) and 3000 fb $^{-1}$  (dashed curves).  $A_{FB}$  reduces the PDF relative uncertainty from 5.4% to 4.5% (4.1%) for a transverse mass of 2 TeV and from 12.9% to 12.5% (11.8%) for a transverse mass of 4 TeV when using an integrated luminosity of 300 (3000) fb $^{-1}$ .  $A_W$  is able to reduce the PDF

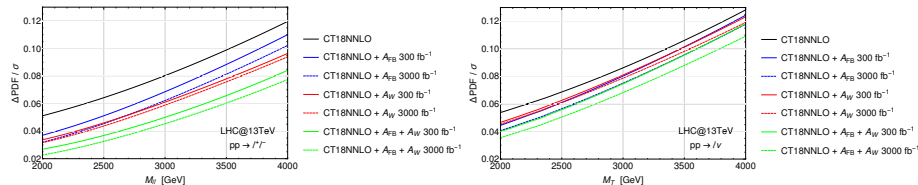


Figure 11: Relative PDF error on the invariant mass spectrum of the neutral DY channel (left) and on the transverse mass spectrum of the charged DY channel (right).

relative uncertainty to 4.7% (4.6%) for a transverse mass of 2 TeV and to 12.3% (11.9%) for a transverse mass of 4 TeV when using an integrated luminosity of 300 (3000)  $\text{fb}^{-1}$ . The combination of  $A_{FB}$  and  $A_W$  data further constrains the PDF relative uncertainty to 4.0% (3.6%) for a transverse mass of 2 TeV and to 11.8% (10.9%) for a transverse mass of 4 TeV when using an integrated luminosity of 300 (3000)  $\text{fb}^{-1}$ .

In the following we will study the impact of the reduction of PDF uncertainties in the invariant mass and transverse mass spectra of specific BSM benchmarks featuring a neutral and charged resonance, respectively. We introduce the enhanced Sequential SM (SSM) model as in Ref. [48], which follows the original SSM [49] and features in its spectrum an extra  $Z'$  and a  $W'$  characterised by the same chiral couplings as the SM gauge bosons, but in this case the overall BSM gauge coupling is enhanced by a factor 3 with respect to the SM one. This is a BSM scenario providing typically wide  $Z'$  ( $\Gamma_{Z'}/M_{Z'} \simeq 27\%$ ) and  $W'$  ( $\Gamma_{W'}/M_{W'} \simeq 41.6\%$ ) whose discovery will occur through (low mass) tail effects rather than on-peak effects. In the following analysis we fix the masses of the neutral and charged heavy gauge bosons to 7.2 TeV and 10 TeV respectively. We will show that the reduction of PDF uncertainties is relevant for an early discovery of their associated signals at the HL-LHC, i.e., for a default luminosity of 3000  $\text{fb}^{-1}$ .

#### 4.2. Effects on $Z'$ searches

The anticipated improvement of the PDFs in the invariant mass spectrum have a substantial impact on searches for BSM neutral resonances. Traditional searches for peaked Breit-Wigner shapes are clearly less concerned by the errors on the PDFs, however, the significance of wide resonance signals is greatly affected by PDF systematic uncertainties. In particular, it has been shown that the presence of a heavy broad resonance can be detected through its interference with the SM background in the invariant mass region below the  $Z'$  mass [48]. Thus, the improvement of the PDF uncertainties in the relevant invariant mass region would considerably enhance the significance of a signal of this kind.

For this purpose, in Fig. 12, we identify the invariant mass region where statistical and PDF uncertainties are comparable. As intimated, here, we have assumed an integrated luminosity of 3000  $\text{fb}^{-1}$  both in the estimation of the statistical errors on the spectrum (red curves) and in the statistical accuracy

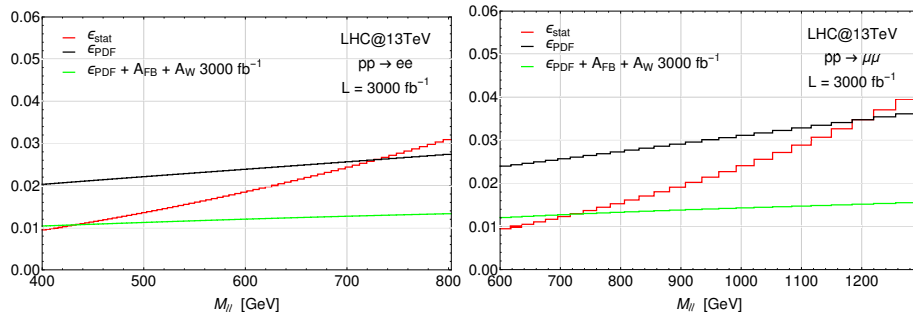


Figure 12: Statistical (red) and PDF uncertainties before (black) and after (green) the profiling in the di-electron (left) and di-muon (right) channels. Experimental resolutions determine the choice of the bin sizes and the experimental efficiency of each channel in the barrel-barrel phase space is also included, as declared by CMS [50].

of the  $A_{FB}$  and  $A_W$  pseudodata included in the profiling of the PDFs (green curves). The two are compared with the original CT18NNLO PDF uncertainty (black curves) in the di-electron (left) and di-muon (right) final states. The choice of the bin sizes in the two plots reflects the different resolutions of the two channels (about 1% for electrons and 3% for the muons) and the estimation of the statistical uncertainties also includes their different efficiencies (about 69% for electrons and 93% for muons in the barrel-barrel phase space), e.g., as reported by CMS [50].

A potential BSM signal in this invariant mass region would then be strongly affected by PDF uncertainties, which the inclusion of  $A_{FB}$  and  $A_W$  data can ameliorate significantly by about a factor 2. To address this effect, we consider the enhanced SSM model introduced in the previous subsection and study its phenomenology in the neutral dilepton channel, where a wide  $Z'$  signal arises. The invariant mass profile, in two specific intervals, of such  $Z'$  realisation is visible in Fig. 13.

Assuming an integrated luminosity of  $3000 \text{ fb}^{-1}$ , the overall significance of the broad peak of a resonance of this kind would be about  $3.2\sigma$ s when including the PDF error, summed in quadrature with the statistical uncertainty, thus at the edge of the sensitivity. The depletion of events due to interference effects that appears below the peak, however, would be statistically significant before the actual observation of the peak itself. Particularly, in the invariant mass region where statistical and PDF uncertainties are comparable, the significance of the depletion of events (assumed here at the same level as an excess of events) would greatly benefit from the foreseen improvement on the PDF error. This is visible in Fig. 14, where the significance of the depletion of events is shown in two invariant mass intervals, for the original CT18NNLO PDF set and for the profiled PDF set using  $A_{FB}$  and  $A_W$  pseudodata with  $3000 \text{ fb}^{-1}$  statistical uncertainty.

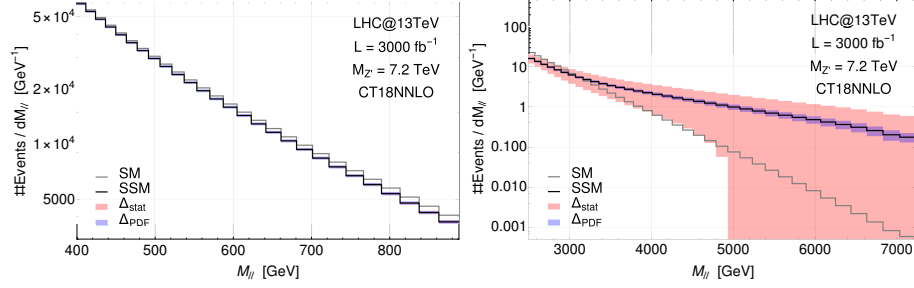


Figure 13: Invariant mass distribution of the number of events for the enhanced SSM  $Z'$  benchmark with a mass of 7.2 TeV. The PDF uncertainty (blue shade) represents the original CT18NNLO error while the statistical error (red shade) corresponds to  $3000 \text{ fb}^{-1}$  of integrated luminosity. NNLO QCD corrections have been applied through a  $K$ -factor. No detector efficiencies are included.

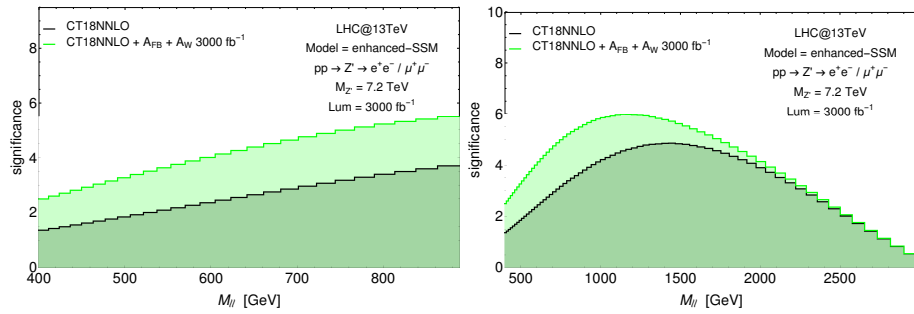


Figure 14: Significance of the enhanced SSM  $Z'$  signal with an integrated luminosity of  $3000 \text{ fb}^{-1}$ , including the PDF error from original CT18NNLO PDF set (black) and after the profiling (green) with  $A_{FB}$  and  $A_W$  pseudodata with the same integrated luminosity accuracy. Efficiencies of both lepton channels are included.

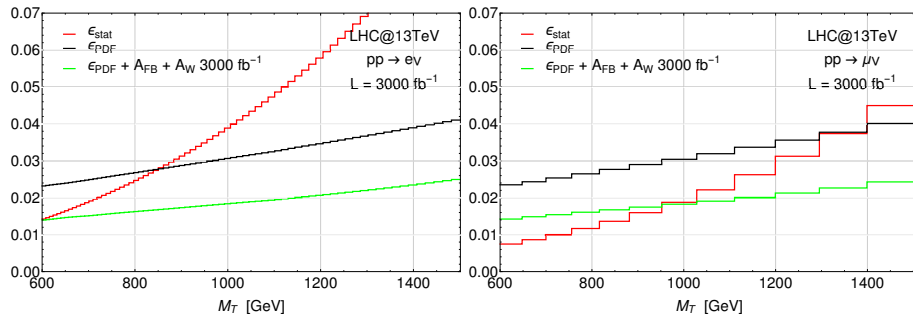


Figure 15: Statistical (red) and PDF uncertainties before (black) and after (green) the profiling in the electron (left) and muon (right) plus missing transverse energy channels. Experimental resolutions determine the choice of the bin sizes and the experimental efficiency of each channel is also included, as declared by ATLAS [51].

#### 4.3. Effects on $W'$ searches

Similar conclusions can be drawn in the charged channel. Fig. 15 shows the comparison between statistical and PDF uncertainties in the transverse mass distribution in the lepton plus missing transverse energy channel. Again, an integrated luminosity of  $3000 \text{ fb}^{-1}$  is assumed in the statistical uncertainty of the spectrum (red curves) and in the accuracy of the  $A_{FB}$  and  $A_W$  pseudodata included in the profiling of the PDFs (green curves). The left (right) plot shows the comparison of the uncertainties in the electron (muon) plus missing transverse energy channel, for which a resolution of about 1.3% (8%) and an efficiency of about 64% (44%) have been assumed, in order to resemble, e.g., the ATLAS experiment features declared in Ref. [51].

The inclusion of  $A_{FB}$  and  $A_W$  data can ameliorate the PDF uncertainty by about a factor 2 and this in turn can significantly improve the experimental sensitivity to  $W'$  states in BSM searches. We study the impact of this effect on the phenomenology of a wide  $W'$  resonance in the enhanced SSM scenario already introduced, for which the transverse mass distribution is visible in Fig. 16.

With an integrated luminosity of  $3000 \text{ fb}^{-1}$ , the broad peak of the chosen benchmark would be below the HL-LHC sensitivity. However, the depletion of events due to interference effects would be visible at an early stage in the low transverse mass tail. In particular, in the transverse mass region where statistical and PDF uncertainties are comparable, the inclusion of  $A_{FB}$  and  $A_W$  pseudodata with  $3000 \text{ fb}^{-1}$  would significantly increase the significance of such a signal (again assumed at the same level as an excess of events), as visible in Fig. 17.

## 5. Conclusions

The main limitation in precision measurements of EW parameters at the various runs of the LHC, including the HL-LHC option, comes from non-perturbative

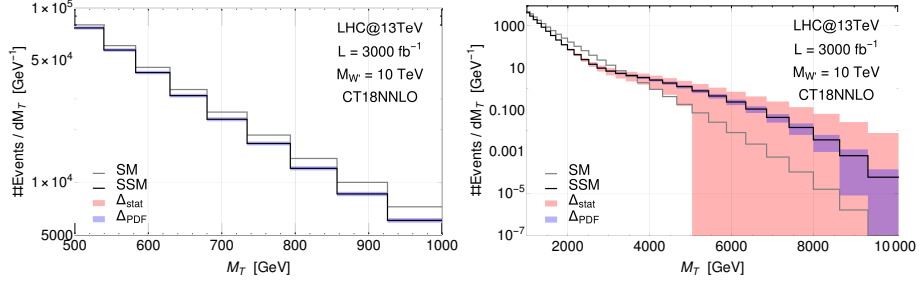


Figure 16: Transverse mass distribution of the number of events for the enhanced SSM  $W'$  benchmark with a mass of 10 TeV. The PDF uncertainty (blue shade) represents the original CT18NNLO error, while the statistical error (red shade) corresponds to  $3000 \text{ fb}^{-1}$  of integrated luminosity. No detector efficiencies are included.

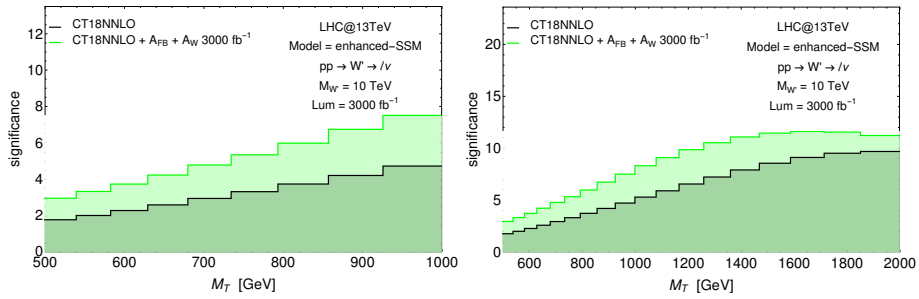


Figure 17: Significance of the enhanced SSM  $W'$  signal with and integrated luminosity of  $3000 \text{ fb}^{-1}$ , including the PDF error from original CT18NNLO PDF set (black) and after the profiling (green) with  $A_{FB}$  and  $A_W$  pseudodata with the same integrated luminosity accuracy. Efficiencies of both lepton channels are included.



PDF uncertainties. These are dealt with in many current analyses by in-situ reweighting and profiling techniques. In this work, we have explored the potential of approaches using the combination of asymmetry measurements in the neutral-current and charged-current DY channels to improve our knowledge of PDFs and reduce the corresponding uncertainties.

While presenting results for a subset of PDFs, we have however verified that the effects described here are of relevance for any PDF set.

Extending the study of Ref. [14] using  $A_{FB}$ , here, we have investigated the impact of combining  $A_{FB}$  with the lepton-charge asymmetry  $A_W$  and shown, by a quantitative analysis using `xFitter`, the complementary constraints provided by the two asymmetries. We have first validated our `xFitter` implementation against ATLAS data at 8 TeV extracting  $A_W$ , finding good  $\chi^2$  values for all the PDF sets examined, and we have then used  $A_{FB}$  and  $A_W$  pseudodata at 13 TeV taken near the vector boson ( $Z$  and  $W$ ) masses to determine the reduction of PDF uncertainties by considering two luminosity scenarios, of  $300 \text{ fb}^{-1}$  (appropriate for Run 3 of the LHC) and  $3000 \text{ fb}^{-1}$  (appropriate for the HL-LHC).

By eigenvector rotation we have illustrated the role of combining  $A_{FB}$  and  $A_W$  in order to place constraints on linearly independent combinations of  $u$  and  $d$  valence quark densities,  $(2/3)u_V + (1/3)d_V$  and  $u_V - d_V$ , respectively, to which the two asymmetries are sensitive at lowest order. Furthermore, we have shown that including  $A_{FB}$  and  $A_W$  in PDF fits reduces the error on the ratio  $\bar{d}/\bar{u}$  at very large  $x$  values, which has been confirmed by several measurements to be much larger than 1 (thereby hinting at a significant flavour asymmetry in the proton sea of antiquarks), to the extent that experimental data are no longer within the error bands predicted by the PDFs.

We have then found that the combined effect of  $A_{FB}$  and  $A_W$  leads to a 30% improvement in the PDF uncertainties on the transverse mass and lepton  $p_T$  distributions in lepton-neutrino final states over a broad kinematic range measured at the LHC around the vector boson peak. In fact, the effect of  $A_W$  alone in the charged DY channel is not dissimilar from that of  $A_{FB}$  in the neutral DY channel, previously seen in the aforementioned reference, so as to suggest that the combined effect of the two asymmetries will also further benefit studies of EW parameters in dilepton final states, chiefly, of  $\sin^2\theta_W$  (this is currently being assessed quantitatively). In fact, we also remark here that the improvement of the PDF uncertainties due to the inclusion of  $A_{FB}$  and  $A_W$  constraints in the mass regions close to  $m_Z$  and  $m_W$ , mapped in the invariant and transverse masses of the neutral and charged channel final states, respectively, may eventually induce a reduction in the error on the determination of  $m_Z$  and  $m_W$  at the (HL-)LHC (and hadron colliders in general). While this may have little phenomenological impact in the case of the  $Z$  mass (which best determination is still given by  $e^+e^-$  data), it may be of relevance for the  $W$  mass (measured more accurately at hadron colliders yet dominated by PDF uncertainties). However, this is beyond the scope of this work and we leave it for a forthcoming publication.

Finally, we have investigated the impact of pseudodata from the peak region

on the description of the high-mass (multi-TeV) region in both the neutral and charged DY channel. We have found that the constraints coming from the  $A_{FB}$  and  $A_W$  combination improve the relative PDF uncertainty by around 20% in the invariant and transverse mass spectra, respectively, between 2 TeV and 4 TeV, a region where evidence of, e.g., wide  $Z'$  and  $W'$  states can first be established.

### **Acknowledgements**

We thank S. Amoroso, S. Camarda and A. Glazov for many useful discussions. FH acknowledges the hospitality and support of DESY, Hamburg and CERN, Theory Division. SM is supported in part through the NExT Institute and acknowledge funding from the STFC Consolidated Grant ST/L000296/1. The work of JF has been supported by STFC under the Consolidated Grant ST/T000988/1. JF and SM acknowledge the use of the IRIDIS High Performance Computing facility, and associated support services, at the University of Southampton, in the completion of this work.

## References

- [1] A. M. Sirunyan, et al., Measurement of the weak mixing angle using the forward-backward asymmetry of Drell-Yan events in pp collisions at 8 TeV, *Eur. Phys. J. C*78 (9) (2018) 701. [arXiv:1806.00863](#), [doi:10.1140/epjc/s10052-018-6148-7](#).
- [2] ATLAS Collaboration, Measurement of the effective leptonic weak mixing angle using electron and muon pairs from  $Z$ -boson decay in the ATLAS experiment at  $\sqrt{s} = 8$  TeV, ATLAS-CONF-2018-037 (2018).
- [3] ATLAS Collaboration, Prospect for a measurement of the Weak Mixing Angle in  $pp \rightarrow Z/\gamma^* \rightarrow e^+e^-$  events with the ATLAS detector at the High Luminosity Large Hadron Collider, ATL-PHYS-PUB-2018-037 (2018).
- [4] Aaboud, M. and others, Measurement of the  $W$ -boson mass in pp collisions at  $\sqrt{s} = 7$  TeV with the ATLAS detector, *Eur. Phys. J. C*78 (2) (2018) 110, [Erratum: *Eur. Phys. J. C*78,no.11,898(2018)]. [arXiv:1701.07240](#), [doi:10.1140/epjc/s10052-018-6354-3](#), [10.1140/epjc/s10052-017-5475-4](#).
- [5] ATLAS Collaboration, Prospects for the measurement of the  $W$ -boson mass at the HL- and HE-LHC, ATL-PHYS-PUB-2018-026 (2018).
- [6] S. Schael, et al., Precision electroweak measurements on the  $Z$  resonance, *Phys. Rept.* 427 (2006) 257–454. [arXiv:hep-ex/0509008](#), [doi:10.1016/j.physrep.2005.12.006](#).
- [7] T. A. Aaltonen, et al., Tevatron Run II combination of the effective leptonic electroweak mixing angle, *Phys. Rev. D*97 (11) (2018) 112007. [arXiv:1801.06283](#), [doi:10.1103/PhysRevD.97.112007](#).
- [8] T. A. Aaltonen, et al., Combination of CDF and D0  $W$ -Boson Mass Measurements, *Phys. Rev. D*88 (5) (2013) 052018. [arXiv:1307.7627](#), [doi:10.1103/PhysRevD.88.052018](#).
- [9] P. Azzi, et al., Report from Working Group 1, CERN Yellow Rep. Monogr. 7 (2019) 1–220. [arXiv:1902.04070](#), [doi:10.23731/CYRM-2019-007.1](#).
- [10] P. Agostini, et al., The Large Hadron-Electron Collider at the HL-LHC, [arXiv:2007.14491](#) (2020). [arXiv:2007.14491](#).
- [11] K. Kovarik, P. M. Nadolsky, D. E. Soper, Hadronic structure in high-energy collisions, *Rev. Mod. Phys.* 92 (4) (2020) 045003. [arXiv:1905.06957](#), [doi:10.1103/RevModPhys.92.045003](#).
- [12] R. Angeles-Martinez, et al., Transverse Momentum Dependent (TMD) parton distribution functions: status and prospects, *Acta Phys. Polon. B*46 (12) (2015) 2501–2534. [arXiv:1507.05267](#), [doi:10.5506/APhysPolB.46.2501](#).

- [13] J. C. Collins, D. E. Soper, G. F. Sterman, Factorization of Hard Processes in QCD, *Adv. Ser. Direct. High Energy Phys.* 5 (1989) 1–91. [arXiv:hep-ph/0409313](#), [doi:10.1142/9789814503266\\_0001](#).
- [14] E. Accomando, et al., PDF Profiling Using the Forward-Backward Asymmetry in Neutral Current Drell-Yan Production, *JHEP* 10 (2019) 176. [arXiv:1907.07727](#), [doi:10.1007/JHEP10\(2019\)176](#).
- [15] S. Alekhin, et al., HERAFitter, *Eur. Phys. J. C* 75 (7) (2015) 304. [arXiv:1410.4412](#), [doi:10.1140/epjc/s10052-015-3480-z](#).
- [16] H. Abdolmaleki, et al., Forward-Backward Drell-Yan Asymmetry and PDF Determination (7 2019). [arXiv:1907.08301](#).
- [17] E. Accomando, J. Fiaschi, F. Hautmann, S. Moretti, Neutral current forward-backward asymmetry: from  $\theta_W$  to PDF determinations, *Eur. Phys. J. C* 78 (8) (2018) 663, [Erratum: *Eur. Phys. J. C* 79, no. 6, 453 (2019)]. [arXiv:1805.09239](#), [doi:10.1140/epjc/s10052-019-6958-2](#), [10.1140/epjc/s10052-018-6120-6](#).
- [18] E. Accomando, J. Fiaschi, F. Hautmann, S. Moretti, Constraining Parton Distribution Functions from Neutral Current Drell-Yan Measurements, *Phys. Rev. D* 98 (1) (2018) 013003, [Erratum: *Phys. Rev. D* 99, no. 7, 079902 (2019)]. [arXiv:1712.06318](#), [doi:10.1103/PhysRevD.98.013003](#), [10.1103/PhysRevD.99.079902](#).
- [19] J. Fiaschi, et al., Constraining PDFs from neutral current Drell-Yan measurements and effects of resummation in slepton pair production (5 2018). [arXiv:1805.00842](#).
- [20] ATLAS Collaboration, Measurement of the cross-section and charge asymmetry of  $W$  bosons produced in proton–proton collisions at  $\sqrt{s} = 8$  TeV with the ATLAS detector, *Eur. Phys. J. C* 79 (9) (2019) 760. [arXiv:1904.05631](#), [doi:10.1140/epjc/s10052-019-7199-0](#).
- [21] A. M. Sirunyan, et al., Measurements of the  $W$  boson rapidity, helicity, double-differential cross sections, and charge asymmetry in  $pp$  collisions at  $\sqrt{s} = 13$  TeV, *Phys. Rev. D* 102 (9) (2020) 092012. [arXiv:2008.04174](#), [doi:10.1103/PhysRevD.102.092012](#).
- [22] Y. Fu, S. Yang, M. Liu, L. Han, T.-J. Hou, C. Schmidt, C. Wang, C. P. Yuan, Reduction of PDF uncertainty in the measurement of the weak mixing angle at the ATLAS experiment (8 2020). [arXiv:2008.03853](#).
- [23] Q. Deng, Q. Han, H. Yin, S. Dulat, T.-J. Hou, C. P. Yuan, Impact of LHCb 13 TeV  $W$  and  $Z$  pseudo-data on the Parton Distribution Functions, *Chin. Phys. C* 45 (2) (2021) 023110. [arXiv:2009.03181](#), [doi:10.1088/1674-1137/abcd90](#).

- [24] T.-J. Hou, Z. Yu, S. Dulat, C. Schmidt, C. P. Yuan, Updating and optimizing error parton distribution function sets in the Hessian approach. II., Phys. Rev. D 100 (11) (2019) 114024. [arXiv:1907.12177](#), [doi:10.1103/PhysRevD.100.114024](#).
- [25] C. Schmidt, J. Pumplin, C. P. Yuan, P. Yuan, Updating and optimizing error parton distribution function sets in the Hessian approach, Phys. Rev. D 98 (9) (2018) 094005. [arXiv:1806.07950](#), [doi:10.1103/PhysRevD.98.094005](#).
- [26] C. Willis, R. Brock, D. Hayden, T.-J. Hou, J. Isaacson, C. Schmidt, C.-P. Yuan, New method for reducing parton distribution function uncertainties in the high-mass Drell-Yan spectrum, Phys. Rev. D 99 (5) (2019) 054004. [arXiv:1809.09481](#), [doi:10.1103/PhysRevD.99.054004](#).
- [27] J. C. Collins, D. E. Soper, Angular Distribution of Dileptons in High-Energy Hadron Collisions, Phys. Rev. D 16 (1977) 2219. [doi:10.1103/PhysRevD.16.2219](#).
- [28] J. Alwall, et al., The automated computation of tree-level and next-to-leading order differential cross sections, and their matching to parton shower simulations, JHEP 07 (2014) 079. [arXiv:1405.0301](#), [doi:10.1007/JHEP07\(2014\)079](#).
- [29] T. Carli, et al., A posteriori inclusion of parton density functions in NLO QCD final-state calculations at hadron colliders: The APPLGRID Project, Eur. Phys. J. C 66 (2010) 503–524. [arXiv:0911.2985](#), [doi:10.1140/epjc/s10052-010-1255-0](#).
- [30] V. Bertone, et al., aMCfast: automation of fast NLO computations for PDF fits, JHEP 08 (2014) 166. [arXiv:1406.7693](#), [doi:10.1007/JHEP08\(2014\)166](#).
- [31] S. Catani, et al., Vector boson production at hadron colliders: a fully exclusive QCD calculation at NNLO, Phys. Rev. Lett. 103 (2009) 082001. [arXiv:0903.2120](#), [doi:10.1103/PhysRevLett.103.082001](#).
- [32] W. Hollik, Radiative Corrections in the Standard Model and their Role for Precision Tests of the Electroweak Theory, Fortsch. Phys. 38 (1990) 165–260. [doi:10.1002/prop.2190380302](#).
- [33] Patrignani, C. et al., Review of Particle Physics, Chin. Phys. C 40 (10) (2016) 100001. [doi:10.1088/1674-1137/40/10/100001](#).
- [34] T.-J. Hou, et al., New CTEQ global analysis of quantum chromodynamics with high-precision data from the LHC, Phys. Rev. D 103 (1) (2021) 014013. [arXiv:1912.10053](#), [doi:10.1103/PhysRevD.103.014013](#).

- [35] S. Bailey, T. Cridge, L. A. Harland-Lang, A. D. Martin, R. S. Thorne, Parton distributions from LHC, HERA, Tevatron and fixed target data: MSHT20 PDFs (12 2020). [arXiv:2012.04684](#).
- [36] R. D. Ball, et al., Parton distributions from high-precision collider data, *Eur. Phys. J. C* 77 (10) (2017) 663. [arXiv:1706.00428](#), [doi:10.1140/epjc/s10052-017-5199-5](#).
- [37] J. Butterworth, et al., PDF4LHC recommendations for LHC Run II, *J. Phys. G* 43 (2016) 023001. [arXiv:1510.03865](#), [doi:10.1088/0954-3899/43/2/023001](#).
- [38] S. Alekhin, J. Blümlein, S. Moch, R. Placakyte, Parton distribution functions,  $\alpha_s$ , and heavy-quark masses for LHC Run II, *Phys. Rev. D* 96 (1) (2017) 014011. [arXiv:1701.05838](#), [doi:10.1103/PhysRevD.96.014011](#).
- [39] H. Abramowicz, et al., Combination of measurements of inclusive deep inelastic  $e^\pm p$  scattering cross sections and QCD analysis of HERA data, *Eur. Phys. J. C* 75 (12) (2015) 580. [arXiv:1506.06042](#), [doi:10.1140/epjc/s10052-015-3710-4](#).
- [40] ATLAS Collaboration, Measurement of the Drell-Yan triple-differential cross section in  $pp$  collisions at  $\sqrt{s} = 8$  TeV, *JHEP* 12 (2017) 059. [arXiv:1710.05167](#), [doi:10.1007/JHEP12\(2017\)059](#).
- [41] S. Amoroso, et al., Longitudinal Z-Boson Polarization and the Higgs Boson Production Cross Section at the Large Hadron Collider (12 2020). [arXiv:2012.10298](#).
- [42] H. Paukkunen, P. Zurita, PDF reweighting in the Hessian matrix approach, *JHEP* 12 (2014) 100. [arXiv:1402.6623](#), [doi:10.1007/JHEP12\(2014\)100](#).
- [43] S. Camarda, et al., QCD analysis of  $W$ - and  $Z$ -boson production at Tevatron, *Eur. Phys. J. C* 75 (9) (2015) 458. [arXiv:1503.05221](#), [doi:10.1140/epjc/s10052-015-3655-7](#).
- [44] J. Pumplin, Data set diagonalization in a global fit, *Phys. Rev. D* 80 (2009) 034002. [arXiv:0904.2425](#), [doi:10.1103/PhysRevD.80.034002](#).
- [45] J. Dove, et al., The asymmetry of antimatter in the proton, *Nature* 590 (7847) (2021) 561–565. [arXiv:2103.04024](#), [doi:10.1038/s41586-021-03282-z](#).
- [46] D. A. Ross, C. T. Sachrajda, Flavor Symmetry Breaking in anti-Quark Distributions, *Nucl. Phys. B* 149 (1979) 497–516. [doi:10.1016/0550-3213\(79\)90004-X](#).
- [47] R. S. Towell, et al., Improved measurement of the anti-d / anti-u asymmetry in the nucleon sea, *Phys. Rev. D* 64 (2001) 052002. [arXiv:hep-ex/0103030](#), [doi:10.1103/PhysRevD.64.052002](#).

- [48] E. Accomando, et al., Production of  $Z'$ -boson resonances with large width at the LHC, *Phys. Lett. B* 803 (2020) 135293. [arXiv:1910.13759](#), [doi:10.1016/j.physletb.2020.135293](#).
- [49] G. Altarelli, B. Mele, M. Ruiz-Altaba, Searching for New Heavy Vector Bosons in  $p\bar{p}$  Colliders, *Z. Phys. C* 45 (1989) 109, [Erratum: *Z.Phys.C* 47, 676 (1990)]. [doi:10.1007/BF01556677](#).
- [50] A. M. Sirunyan, et al., Search for high-mass resonances in dilepton final states in proton-proton collisions at  $\sqrt{s} = 13$  TeV, *JHEP* 06 (2018) 120. [arXiv:1803.06292](#), [doi:10.1007/JHEP06\(2018\)120](#).
- [51] ATLAS Collaboration, Search for a heavy charged boson in events with a charged lepton and missing transverse momentum from  $pp$  collisions at  $\sqrt{s} = 13$  TeV with the ATLAS detector, *Phys. Rev. D* 100 (5) (2019) 052013. [arXiv:1906.05609](#), [doi:10.1103/PhysRevD.100.052013](#).